Research Square

Preprints are preliminary reports that have not undergone peer review.
They should not be considered conclusive, used to inform clinical practice,
or referenced by the media as validated information.

Quantitative Assessment of Regional Aerosol Deposition and Early Airway Clearance Using [18F]NaF Nebulized Inhalation PET/CT

Xinlu Zhang
First Affiliated Hospital of Guangzhou Medical University
Ruiyue Zhao
First Affiliated Hospital of Guangzhou Medical University
Shaoyu Liu
First Affiliated Hospital of Guangzhou Medical University
Yu Wang
First Affiliated Hospital of Guangzhou Medical University
Ziqi Zhang
First Affiliated Hospital of Guangzhou Medical University
Shaonan Zhong
First Affiliated Hospital of Guangzhou Medical University
Xiang Yan
First Affiliated Hospital of Guangzhou Medical University
Zeguang Zheng
First Affiliated Hospital of Guangzhou Medical University
Nanshan Zhong
First Affiliated Hospital of Guangzhou Medical University
Linling Cheng
First Affiliated Hospital of Guangzhou Medical University
Xinlu Wang
71lu@163.com

First Affiliated Hospital of Guangzhou Medical University https://orcid.org/0000-0003-1997-5687

Research Article

Keywords: Methodological, Quantitative, Aerosolized radiopharmaceutical, PET/CT, Lung disease

Posted Date: June 28th, 2026

DOI: https://doi.org/10.21203/rs.3.rs-9806381/v1

License: This work is licensed under a Creative Commons Attribution 4.0 International License.
Read Full License

Abstract

Objective

To visualize and quantify regional pulmonary aerosol deposition and early airway clearance using aerosolized [^{18}F]NaF PET/CT in bronchiectasis.

Methods

In this prospective study, 77 adults with CT-confirmed bronchiectasis underwent aerosolized [^{18}F]NaF PET/CT. Regional deposition in bronchiectatic versus healthy lung was assessed on the 0-min scan using target-to-blood ratio (TBR) and total deposited activity. Deposition robustness was evaluated across different nebulizer types. A subgroup underwent dynamic imaging (0–30 min) followed by serial static scans up to 120 min, with kinetic analysis using a dual-pathway clearance model.

Results

The 0-min PET/CT demonstrated visually apparent photopenic defects in bronchiectatic regions. Quantitatively, bronchiectatic lung showed significantly lower deposition than healthy lung (TBR: 1.30 [0.63–1.58] vs. 2.30 [1.60–2.65]; $p < 0.05$) and markedly reduced total activity (43.18 [5.7–47.08] vs. 1413.33 [581.95–2155.68]; $p < 0.0001$). These findings were consistent across all nebulizer systems. Dynamic imaging showed early clearance was dominated by mucociliary transport (kmc > kabs), with minimal systemic absorption. Serial imaging (0–120 min) showed no increase in bronchiectatic activity, while healthy lung activity declined gradually, indicating 0 min as the optimal time point for deposition assessment. Bronchodilator administration did not alter clearance kinetics in bronchiectatic regions.

Conclusion

Aerosolized [^{18}F]NaF PET/CT enables quantitative assessment of regional aerosol deposition and airway clearance in bronchiectasis, revealing persistent deposition deficits in diseased airways and mucociliary-dominant early clearance with minimal systemic absorption.

Introduction

Inhalation therapy plays a central role in the management of chronic respiratory diseases, enabling direct drug delivery to the airways while minimizing systemic exposure[1, 2]. However, clinical effectiveness depends not only on the administered dose but also on the efficiency and regional distribution of pulmonary aerosol deposition[3]. In routine practice, inhaled drug delivery remains largely invisible, as assessment relies predominantly on indirect metrics—such as spirometry or symptom scores—which fail

to provide spatial information on where aerosolized droplets actually deposit and accumulate within the complex architecture of the respiratory tract.

Current imaging technology cannot fill this gap. High-resolution computed tomography (HRCT) details structural airway abnormalities but cannot trace aerosol distribution [4, 5], whereas hyperpolarized ^{129}Xe MRI[6–8] and nuclear medicine ventilation scintigraphy[9, 10] modalities are generally restricted to qualitative planar analysis with poor spatial resolution. More importantly, gases and nanometer-sub-micron particles are designed to strictly follow airflow to the alveoli, failing to replicate the aerodynamic behavior—such as inertial impaction in the central airways—of therapeutic-sized aqueous droplets (> 3 μm). Thus, a significant gap remains in accurately modeling true inhaled drug delivery.

Positron emission tomography (PET) offers distinct advantages for quantitative assessment of pulmonary aerosol deposition due to its high sensitivity, three-dimensional tomographic capability, and intrinsic quantitative potential[11–13]. Although the feasibility of aerosol PET imaging has been demonstrated using various positron-emitting tracers and inhalation strategies[14–17], existing studies have largely been limited to global lung measurements, without region-specific quantification of deposition patterns or systematic evaluation of aerosol clearance dynamics. Airway diseases such as bronchiectasis, marked by pronounced structural abnormalities and spatial heterogeneity[2, 18], provide a suitable model to evaluate the robustness of quantitative aerosol PET frameworks under clinically relevant conditions[19]. For this purpose, ^{18}F-sodium fluoride ([^{18}F]NaF) serves as an ideal surrogate tracer; its poor epithelial permeability ensures it remains trapped in the airway surface liquid, strictly tracing mechanical mucociliary clearance without confounding systemic absorption[20]. In addition, as a dissolved ionic tracer delivered in aqueous solution, [^{18}F]NaF closely mimics the solvent phase of clinically nebulized medications, more faithfully representing the deposition behavior of drug-containing droplets within the airway surface liquid. [^{18}F]NaF PET emerges as a promising imaging modality to address the a forementioned limitations, offering unique advantages for quantitative assessment of pulmonary aerosol deposition.

Accordingly, the present study aimed to preliminarily explore a PET/CT-based approach for quantifying regional aerosol deposition and early-stage clearance kinetics following nebulized inhalation. By leveraging this imaging strategy, we sought to evaluate the actual in vivo delivery and spatial distribution of therapeutic-sized aerosols within the lungs, thereby establishing an imaging-based framework for assessing inhaled drug transport and airway clearance dynamics.

Materials and Methods

1.1 Study Design and Population

This prospective, observational methodological study was designed to develop and validate a standardized PET/CT-based framework for the quantitative assessment of intrapulmonary aerosol

deposition using [^{18}F]NaF. The study protocol was approved by the Institutional Review Board (Ethics Committee) of the First Affiliated Hospital of Guangzhou Medical University (Approval No: ES-2024-119-01). Written informed consent was obtained from all participants prior to enrollment.

Adult patients (aged 18–85 years) with suspected or confirmed bronchiectasis, diagnosed via clinical assessment and high-resolution computed tomography (HRCT)[21], were prospectively enrolled. Patients were required to be capable of completing spirometry, aerosol inhalation, and subsequent PET/CT imaging. Key exclusion criteria included: (1) inability to tolerate the inhalation procedure or spirometry; (2) pregnancy or breastfeeding; (3) severe cardiopulmonary impairment precluding safe PET/CT scanning; (4) known hypersensitivity or intolerance to nebulized agents; and (5) any other conditions deemed by the investigators to compromise protocol compliance or patient safety.

1.2 Radiopharmaceutical Preparation

^{18}F-fluoride was produced via the ^{18}O(p,n)^{18}F nuclear reaction using a GE PETtrace 860 cyclotron (GE Healthcare). The aqueous solution was trapped on a Sep-Pak Light QMA cartridge (Waters) pre-conditioned with 0.5 M $NaHCO_3$ and sterile water, followed by elution with 2 mL of physiological saline. The final [^{18}F]NaF solution, formulated to a target activity of approximately 370 MBq (10 mCi), was passed through a 0.22 μm filter to ensure sterility. Radiochemical purity (> 95%) and visual appearance were verified according to standard institutional quality control procedures prior to administration.

1.3 Aerosol Administration Protocol

Aerosol delivery of the [^{18}F]NaF solution was performed using one of the following nebulizer systems depending on device availability at the time of imaging: a jet nebulizer (OMRON NE-C28, Japan), a mesh nebulizer (Air Pro 6+, Feellife, China), or an ultrasonic nebulizer (Air 360 mini + E, Feellife, China).

For each participant, 2 mL of the prepared [^{18}F]NaF saline solution (370 MBq) was loaded into the nebulizer chamber. The nebulization process was characterized by a mass median aerodynamic diameter (MMAD) of approximately 3 μm and an inhalation flow of 20 L/min. Participants, seated upright, were instructed to inhale the aerosol using tidal breathing through a securely sealed mouthpiece while employing a nose clip to prevent nasal breathing. The total inhalation duration was strictly controlled at 5 minutes (approximately 30 respiratory cycles). To prevent interaction or altered deposition, [^{18}F]NaF aerosol was administered independently and was not mixed with any routine clinical inhaled medications(Fig. 1).

1.4 PET/CT Acquisition and Reconstruction

All imaging was performed on an integrated PET/CT system (Discovery MI, GE Healthcare). At 5 minutes post-inhalation, participants were positioned supine for a static whole-lung scan. A low-dose CT was first acquired for attenuation correction and anatomical localization (parameters: 80 kV, 150 mA, pitch 1.675, rotation time 0.5 s, reconstructed to a slice thickness of 2.5 mm for the lungs and 3.75 mm globally).

The static PET emission scan was then acquired at 2 minutes per bed position, covering from the oropharynx to the upper abdomen. Immediately after completion of the initial static scan, a 30-min dynamic PET acquisition was initiated to characterize clearance kinetics, comprising 30 frames (12 × 15 s, 2 × 30 s, 6 × 60 s, and 10 × 120 s). Subsequently, a subset of participants underwent additional delayed static PET acquisitions using the same whole-lung protocol at predefined time points.

1.5 Image Processing and Volume of Interest (VOI) Definition

Image co-registration and VOI delineations were performed using 3D Slicer (version 5.10.0). Initially, whole-lung and primary airway masks were automatically segmented from the low-dose CT images utilizing TotalSegmentator (v2)[22]. To optimize airway continuity, Hounsfield Unit (HU)-based thresholding coupled with connected-component analysis was applied within the lung mask to isolate the complete intrathoracic airway tree. The carina and the distal endpoints of the main bronchi served as anatomical reference points.

Subsequently, targeted VOIs were manually delineated by two experienced nuclear medicine physicians, with any inter-observer discrepancies resolved by consensus. Bronchiectatic regions were defined on CT as areas exhibiting evident bronchial dilatation and wall thickening. Conversely, Healthy lung regions were identified as areas with preserved parenchymal architecture and no radiologic signs of bronchiectasis.

1.6 Quantitative Metrics

Voxel-wise standardized uptake values (SUV) were extracted from the co-registered PET images. Tracer deposition was quantified using a target-to-blood ratio (TBR) to normalize for systemic vascular background. TBR was defined as the SUVmean of the target VOI divided by the SUVmean of the descending aorta blood pool. To ensure measurement consistency and minimize partial volume effects from the vessel wall, the aortic blood pool activity was determined by manually placing a standardized spherical VOI (2.0 cm in diameter) centrally within the lumen of the descending thoracic aorta on the fused PET/CT images.

Furthermore, total regional aerosol deposition was estimated by multiplying the SUVmean by the corresponding VOI volume (cm^3).

1.7 Kinetic Analysis and Clearance Modeling

Time-activity curves (TACs) were extracted from the dynamic PET data for the healthy lung, bronchiectatic areas, and the T10 vertebral cancellous bone. For each VOI at frame time $\mathbf{t_i}$, the total clearance rate ($\mathbf{k_{tot}}$) was estimated using a post-peak mono-exponential decay model. Only data points following the peak activity time ($t \geq t_0$) were included in the fitting process:

$$A_{ROI}(t) = A_0 e^{-k_{tot} \cdot |t - t_0|}$$

A weighted least-squares linear regression of lnA_{ROI} against (t-t_0) in minutes was performed, utilizing the frame duration (Δt) as weights (w_i = Δt). The k_{tot} was derived as the negative slope of this regression.

To isolate the mucociliary clearance component, the apparent systemic absorption rate (**k_{abs}**) was derived. The T10 vertebral cancellous bone was employed as an output proxy (sink) for blood-borne ^{18}F-fluoride absorbed from the lungs. The net accumulation of activity in the bone (ΔA_{bone}) from the peak time (t_0) to the end of the dynamic acquisition (t_{end}) was calculated as:

$$\Delta A_{bone} = A_{bone}(t_{end}) - A_{bone}(t_0)$$

The cumulative exposure in the pulmonary region was represented by the area under the curve (AUC_{VOI}) of the corresponding lung VOI, computed via discrete integration:

$$AUC_{VOI} = \sum A_{VOI}(t_i)\Delta t_i$$

Subsequently, the apparent systemic absorption rate (**k_{abs}**) was calculated as the ratio of the net bone accumulation to the pulmonary cumulative exposure:

$$k_{abs} = \frac{\Delta A_{bone}}{AUC_{ROI}}$$

Finally, assuming that the total clearance is the sum of mucociliary transport and systemic absorption, the mucociliary clearance rate (**k_{mc}**) for the pulmonary VOIs was determined by subtracting the systemic absorption component from the total clearance:

$$k_{mc} = k_{tot} - k_{abs}$$

1.8 Statistical analysis

Statistical analyses were performed using IBM SPSS Statistics (version 26; IBM Corp.) and GraphPad Prism (version 6). Continuous variables are presented as mean ± SD for approximately normally distributed data and as median (IQR) for non-normally distributed data. Normality was assessed using the Shapiro–Wilk test. For between-group comparisons, Welch's t-test was applied when normality assumptions were met; otherwise, the Mann–Whitney U test was used. All tests were two-tailed, and $P < 0.05$ was considered statistically significant.

Results

2.1 Study population and baseline characteristics

Between March 2022 and November 2025, a total of 77 patients with bronchiectasis who met the eligibility criteria were enrolled and underwent aerosolized [^{18}F]NaF PET/CT imaging (Fig. 2). Based on

the nebulizer system utilized, the cohort was stratified into three groups: a mesh nebulizer group (n = 11), an ultrasonic nebulizer group (n = 9), and a jet nebulizer group (n = 57). To further evaluate the effect of airway interventions, patients within the jet nebulizer cohort were assigned to either a saline control group (n = 27) or a saline plus bronchodilator group (n = 30).

The baseline demographic and clinical characteristics of the study population are summarized in Table 1. The cohort was predominantly female (77.9%, 60/77), with an overall median age of 42.8 years (IQR: 26.0–59.0) and a median body mass index (BMI) of 19.9 kg/m^2 (IQR: 18.1–22.0), reflecting a generally lean physique typical of patients with bronchiectasis. Baseline spirometry revealed mild-to-moderate airflow impairment, characterized by a median FEV_1 of 71.8% predicted (IQR: 59.4–84.4), an FVC of 84.9% predicted (IQR: 77.3–96.6), and an FEV_1/FVC ratio of 84.9% (IQR: 78.0–97.9).

Table 1
Baseline characteristics of bronchiectasis patients undergoing aerosolized [^{18}F]NaF PET/CT

Characteristic	Overall (n = 77)
Sex, n (%)	
Male	17 (22%)
Female	60 (78%)
Age (years)	42.8(26.0–59.0)
BMI (kg/m^2)	19.9 (18.1–22.0)
Baseline spirometry	
FEV_1 (% predicted)	71.8(59.4–84.4)
FVC (%)	84.9(77.3–96.6)
FEV1/FVC (%)	84.9(78.0-97.9)

Abbreviations: BMI, body mass index; FEV_1, forced expiratory volume in 1 second; FVC, forced vital capacity.

Data are expressed as median (interquartile range) for continuous variables and as number (percentage) for categorical variables.

2.2 Impaired regional deposition of aerosolized [^{18}F]NaF in bronchiectatic lung regions

On qualitative assessment, aerosolized [^{18}F]NaF PET/CT demonstrated heterogeneous pulmonary tracer distribution. Visually, tracer activity was substantially reduced within bronchiectatic regions compared to

the adjacent, morphologically healthy lung parenchyma (Fig. 3A). The qualitative identification of these deposition-deficient regions showed high inter-reader agreement, yielding an overall concordance rate of 93.5%. This pattern was consistently observed in both regional and diffuse bronchiectasis, where bronchiectatic segments (red arrows) showed relatively lower tracer signal than reference healthy regions (green dashed circles).

Quantitatively, the TBR was significantly lower in bronchiectatic regions than in healthy regions (1.30[0.63, 1.58] vs 2.30[1.60, 2.65]; Fig. 3B). Similarly, the total regional aerosol deposition was markedly reduced in bronchiectatic regions compared with healthy regions (43.18[5.7, 47.08] vs 1413.33[581.95, 2155.68]; Fig. 3B). These quantitative metrics strongly support the premise of impaired aerosol delivery and localized ventilation deficits within bronchiectatic airways.

2.3 Consistent impairment of aerosol deposition in bronchiectatic VOIs across delivery conditions

To assess the robustness of regional signal differences under varying inhalation conditions, TBR was compared between healthy lung regions and bronchiectatic regions across nebulization regimens and nebulizer types (Fig. 4).

Within the jet nebulizer cohort, the structural deposition barriers in diseased airways remained prominent regardless of pretreatment. Specifically, in both the saline-only and the saline plus bronchodilator regimens, bronchiectatic VOIs consistently exhibited significantly lower tracer uptake than paired healthy VOIs (all $P < 0.05$; Fig. 4A). The relative deposition efficiency, expressed as the bronchiectasis-to-healthy TBR ratio, remained consistently low [median ratio: *0.63* vs. *0.66*, respectively], indicating that bronchodilator administration could not reverse the localized aerosol penetration failure.

Furthermore, stratification by aerosol generation mechanism yielded an identical pattern. Across mesh, ultrasonic, and jet nebulizers, tracer deposition was persistently attenuated in bronchiectatic volumes relative to healthy regions (all $P < 0.05$; Fig. 4B). The comparable TBR ratios across the three devices (Fig. 4B, right panel) further validate that the impaired regional delivery is a disease-specific anatomical and physiological consequence, rather than an artifact of the nebulization physics or specific inhalation device used.

2.4 Spatiotemporal kinetics and delayed retention of aerosolized [^{18}F]NaF

To evaluate early clearance kinetics and delayed tracer retention, a combined dynamic and static PET/CT protocol was performed in a subgroup of 10 patients (Fig. 5A). Using blood-pool-normalized TBR, the generated time-activity curves (TACs) revealed distinct spatiotemporal profiles across different pulmonary structures (Fig. 5B). The central airways exhibited the highest initial activity followed by a rapid exponential decline, consistent with the rapid mucociliary clearance of proximally deposited larger

particles. Conversely, the healthy lung parenchyma displayed lower initial uptake with a much more gradual clearance slope.

Strikingly, bronchiectatic VOIs consistently demonstrated the lowest TBR from the initial dynamic phase through the entire observation period. Serial static scanning at 30, 60, 90, and 120 min post-inhalation confirmed the persistence of this hierarchical regional pattern (central airways > healthy parenchyma > bronchiectasis) across all delayed time points. Furthermore, when comparing inhalation regimens in patients with preserved to mildly impaired ventilatory function, neither saline alone nor saline plus bronchodilator significantly altered the regional TBR kinetics (Fig. 5C), indicating that acute bronchodilator administration does not influence macroscopic aerosol distribution over time.

2.5 Dual-pathway clearance modeling and quantification

A dual-pathway, first-order kinetic model was applied to the 0–30 min dynamic PET data to partition the total clearance rate (k_{tot}) into mucociliary clearance (k_{mc}) and systemic blood absorption (k_{abs}) components (Fig. 6A). Dynamic tracking of the total regional deposition (SUVmean × volume) re-emphasized that tracer accumulation remained severely blunted in bronchiectatic VOIs compared to healthy lung parenchyma throughout the entire early dynamic window (Fig. 6B).

Quantitative model estimates revealed that mucociliary transport (k_{mc}) was the predominant driver of early post-inhalation clearance, whereas the systemic absorption component (k_{abs}) was negligible across all pulmonary regions. Importantly, no significant differences in k_{tot}, k_{mc}, or k_{abs} were observed between the saline and saline plus bronchodilator regimens, neither in the healthy lung nor in the bronchiectatic VOIs (Table 2). Collectively, these findings demonstrate that the early signal decay is governed almost exclusively by airway mucus transport, and that the profound deposition deficit within bronchiectatic airways persists regardless of bronchodilator intervention.

Table 2
Model-derived regional clearance rate constants: saline versus saline plus bronchodilator regimen

($\times 10^{-3}$ min^{-1})	Saline Group	Saline + Bronchodilator Group	*P*
Healthy			
k_{tot} ($\times 10^{-3}$ min^{-1})	23.85 ± 5.96	29.07 ± 6.87	0.237
k_{abs} ($\times 10^{-3}$ min^{-1})	0.19 ± 0.25	0.23 ± 0.09	0.222
k_{mc} ($\times 10^{-3}$ min^{-1})	23.66 ± 6.12	28.83 ± 6.93	0.246
Bronchiectasis			
k_{tot} ($\times 10^{-3}$ min^{-1})	21.50 ± 8.41	16.44 ± 6.64	0.323
k_{abs} ($\times 10^{-3}$ min^{-1})	0.18 ± 0.25	0.23 ± 0.09	0.151
k_{mc} ($\times 10^{-3}$ min^{-1})	21.33 ± 8.54	16.22 ± 6.70	0.325
(mean ± SD; between-regimen P values shown).			

Discussion

In this methodological study, we established a quantitative PET/CT framework to directly visualize the spatial deposition and early clearance kinetics of aerosolized radiopharmaceuticals. By applying this approach to a cohort of patients with bronchiectasis, we demonstrated the feasibility of tracking therapeutic-sized aerosols in structurally remodeled airways. Rather than reiterating specific numerical outcomes, this study highlights a paradigm shift: our framework delineates the true delivery patterns of inhaled agents and quantitatively distinguishes airway mucociliary transport from systemic absorption, providing a robust, non-invasive tool for evaluating inhaled drug efficiency and localized clearance dysfunction.

A major methodological advantage and conceptual innovation of our approach is its ability to directly visualize the spatial fate of therapeutic-sized aerosols, which provides insights fundamentally distinct from traditional ventilation scintigraphy. Conventional ventilation imaging (e.g., using Technegas or radioactive gases) utilizes submicron particles or inert gases designed to evade airway deposition and reach the alveoli, thereby reflecting pure regional airflow[19, 23]. In contrast, our nebulized [^{18}F]NaF solution generates larger droplets (mass median aerodynamic diameter 3 μm) that closely mimic the physical behavior of actual inhaled therapeutics. Consequently, our PET/CT framework maps true drug delivery patterns. In structurally remodeled bronchiectatic airways, the combination of airway dilation, mucus hypersecretion, and altered airflow creates turbulence[24]. These aerodynamic perturbations

cause therapeutic-sized particles to deposit prematurely in the central or proximal airways via inertial impaction, failing to penetrate into the distal parenchymal segments[3]. Consistent with this mechanism, tracer deposition in healthy lung regions peaked immediately post-inhalation (0 min), whereas bronchiectatic regions exhibited persistently low deposition during all subsequent time points, underscoring a stable regional delivery dificit rather than a transient kinetic effect. Regrettably, this finding confirms that structurally abnormal airways—the primary targets for inhaled therapies—are systematically disadvantaged in receiving aerosolized medications.

The robustness of this deposition defect across both technical and pharmacologic conditions further underscores the underlying pathophysiology of the disease. Specifically, the persistently lower target-to-background ratio (TBR) in bronchiectatic regions across mesh, ultrasonic, and jet nebulizers confirms a true biological barrier rather than a device-specific artifact. Importantly, the inability of acute bronchodilator administration to improve regional deposition or alter clearance kinetics underscores that bronchiectasis is characterized by rigid, irreversible structural remodeling and mucus plugging—distinct from the reversible smooth muscle bronchospasm observed in asthma

Inhaled [^{18}F]fluorodeoxyglucose ([^{18}F]FDG) has been employed in clinical investigations to map and quantify the spatial heterogeneity of aerosol deposition throughout the human respiratory tract. This approach entails radiolabeling nebulized solutions or dry-powder inhaler formulations with [^{18}F]FDG, thereby enabling non-invasive, quantitative tracking of inhaled particles via PET. Relative to conventional gamma scintigraphy which typically utilizes technetium-99m-labeled aerosols, [^{18}F]FDG PET affords superior spatial resolution, enhanced signal-to-noise characteristics, and robust quantitative capabilities. These advantages derive from favorable nuclear properties, such as a 109.8-minute physical half-life, high positron abundance (97%), and relatively low positron energy (mean 250 keV), all of which facilitate accurate dynamic imaging and compartmental kinetic modeling.

Nevertheless, a fundamental limitation stems from the intrinsic biochemical behavior of [^{18}F]FDG. As a glucose analogue, it enters cells predominantly via facilitative glucose transporters (GLUT1 and GLUT3) and undergoes phosphorylation by hexokinase to [^{18}F]FDG-6-phosphate, a metabolite that cannot proceed further in glycolysis and therefore accumulates intracellularly in proportion to local hexokinase activity and glucose metabolic rate. Consequently, radiotracer accumulation reflects not only the physical distribution of deposited aerosol, but also regional variations in cellular metabolism. In pulmonary tissue, this results in elevated uptake at sites of heightened metabolic activity, including active infectious foci (e.g., bacterial pneumonia, mycobacterial infection), inflammatory infiltrates (e.g., during asthma or chronic obstructive pulmonary disease exacerbations, granulomatous inflammation in sarcoidosis), and neoplastic lesions (e.g., primary non-small cell lung cancer or pulmonary metastases). Thus, focal increases in [^{18}F]FDG PET may represent pathological metabolic activity rather than actual aerosol retention, introducing interpretive ambiguity when characterizing deposition patterns and assessing inhaler performance.

In contrast, [^{18}F]sodium fluoride ([^{18}F]NaF) offers several distinct advantages for aerosol deposition studies. Firstly, dissolved in sodium chloride solution, [^{18}F]NaF functions as a direct radiolabeling agent for nebulized saline or hypertonic saline, preserving the original formulation composition with minimal alteration. Unlike [^{18}F]FDG, which may interfere with drug-excipient interactions, [^{18}F]NaF integrates seamlessly into standard clinical aerosol preparations, preserving the physicochemical properties of the original therapeutic formulation. Secondly, [^{18}F]NaF does not undergo cellular uptake via glucose transporters or hexokinase-mediated phosphorylation; its deposition pattern reflects purely physical aerosol distribution without confounding metabolic accumulation. Consequently, focal signal increases unambiguously indicate actual particle retention rather than pathological hypermetabolism, eliminating interpretive uncertainty in the presence of infection, inflammation, or malignancy. This property ensures that regional PET signal intensity correlates exclusively with deposited aerosol mass, enabling accurate assessment of inhaler performance, airway penetration, and ventilation heterogeneity irrespective of underlying pulmonary pathology. Thirdly, [^{18}F]NaF may be less prone to early trans-epithelial diffusion. Consistent with this property, our dynamic modeling demonstrated that the apparent systemic absorption rate (kabs) of [^{18}F]NaF was negligible during the first 30 minutes, supporting its confinement to the airway surface liquid and mucus layer. Consequently, early signal decay predominantly reflects mechanical mucociliary clearance (k_{mc}), providing a more physiologically specific surrogate for quantifying airway clearance dynamics.

Validating that [^{18}F]NaF PET/CT accurately reflects true airway mucus transport capacity opens several clinically relevant applications. First, these quantitative deposition and kinetic metrics can serve as specific functional biomarkers to stratify bronchiectasis phenotypes (e.g., mucus-dominant vs. non-mucus-dominant) and act as pharmacodynamic endpoints in trials evaluating mucoactive agents, inhaled antibiotics, or chest physiotherapy. Second, patient- and region-specific mapping of aerosol deposition can directly inform rational delivery strategies, guiding nebulizer device selection and personalized inhalation coaching. Finally, this quantitative framework can be readily extended to other obstructive diseases characterized by heterogeneous ventilation and mucus plugging, such as chronic obstructive pulmonary disease (COPD) and cystic fibrosis.

Study limitations

Several limitations warrant consideration. The dynamic kinetic analysis was confined to a small subgroup, limiting power to detect subtle regimen effects and to support subgroup analyses. Nebulizer type and inhalation regimen were not randomized, and residual confounding cannot be excluded. Quantitative deposition may be affected by motion, partial-volume effects. The clearance model applies simplifying assumptions and the 0–30 min window may miss slower clearance components.

Conclusion

In summary, PET/CT imaging after aerosolized radiopharmaceutical administration enables direct visualization and quantification of regional deposition and early clearance.In patients with bronchiectasis, aerosol deposition in bronchiectatic lung regions is consistently reduced. This reduced deposition remains stable regardless of the nebulizer device or inhalation regimen used, and persists over time. Additionally, early clearance of the aerosol is mainly driven by mucociliary transport. Specifically, these findings strengthen the feasibility and translational potential of this approach as a quantitative tool for evaluating aerosol delivery and airway clearance dysfunction in pulmonary disease.

Declarations

Ethics approval and consent to participate

All procedures involving human participants were performed in accordance with the ethical standards of the institutional and/or national research committee, as well as the 1964 Helsinki Declaration and its later amendments or comparable ethical standards. Informed consent was obtained from all individual participants included in the study.

Consent for publication

Written informed consent for publication was obtained from all participants.

Availability of data and material

The datasets generated and/or analyzed during the current study are available from the corresponding author upon reasonable request.

Competing interests

No other potential conflict of interest relevant to this article was reported.

Funding

Not applicable.

Authors' contributions

Xinlu Wang, Linling Cheng, Nanshan Zhong, and Zeguang Zheng conceived and designed the study. Yu Wang and Ziqi Zhang recruited the participants and collected the clinical data. Xinlu Zhang, Shaonan Zhong, and Xiang Yan performed the imaging procedures and image analysis. Xinlu Zhang and Ruiyue Zhao analyzed and interpreted the data. Xinlu Zhang drafted the manuscript. Shaoyu Liu, Xinlu Wang, and Ruiyue Zhao critically revised the manuscript for important intellectual content. All authors read and approved the final manuscript.

Acknowledgements

The authors thank all participants who took part in this study. The authors also thank the clinical, technical, and research staff of the First Affiliated Hospital of Guangzhou Medical University for their support during participant recruitment, imaging acquisition, and data collection.

List of Supplementary Materials

Schematic of Target Delineation in Bronchiectasis Regions；Inter-reader concordance for qualitative identification of bronchiectatic regions on aerosolized [^{18}F]NaF PET/CT

References

1. SCHEUCH G, KOHLHAEUFL M J, BRAND P, et al. Clinical perspectives on pulmonary systemic and macromolecular delivery [J]. Adv Drug Deliv Rev. 2006;58(9–10):996–1008.
2. CHALMERS JD, CHANG A B, CHOTIRMALL S H, et al. Bronchiectasis [J]. Nat Rev Dis Primers. 2018;4(1):45.
3. DARQUENNE C. Aerosol deposition in health and disease [J]. J Aerosol Med Pulm Drug Deliv. 2012;25(3):140–7.
4. COXSON HO. Quantitative computed tomography assessment of airway wall dimensions: current status and potential applications for phenotyping chronic obstructive pulmonary disease [J]. Proc Am Thorac Soc. 2008;5(9):940–5.
5. COZZI D, GOZZI L, GIOVANNELLI S, et al. Back to the future in asthma imaging: quantitative assessment and new perspectives [J]. Radiol Med; 2025.
6. ELBEHAIRY A F, MARSHALL H, NAISH JH et al. Advances in COPD imaging using CT and MRI: linkage with lung physiology and clinical outcomes [J]. Eur Respir J, 2024, 63(5).
7. HAHN A D, CAREY K J, BARTON G P, et al. Hyperpolarized (129)Xe MR Spectroscopy in the Lung Shows 1-year Reduced Function in Idiopathic Pulmonary Fibrosis [J]. Radiology. 2022;305(3):688–96.
8. MACLEOD JL, KHAN H M FRANKLINA et al. Hyperpolarized Xenon-129 MRI: Narrative Review of Clinical Studies, Testing, and Implementation of Advanced Pulmonary In Vivo Imaging and Its Diagnostic Applications [J]. Diagnostics (Basel), 2025, 15(4).
9. PARTHIPUN A, GOPALAN D. GIBBS S, et al. Clinical guideline for ventilation-perfusion scintigraphy in pulmonary hypertension [J]. Nucl Med Commun; 2025.
10. PEIFFER JD, ALTES T, RUSET I C, et al. Hyperpolarized (129)Xe MRI, (99m)Tc scintigraphy, and SPECT in lung ventilation imaging: a quantitative comparison [J]. Acad Radiol. 2024;31(4):1666–75.
11. CHEN D L, CHERIYAN J, CHILVERS E R, et al. Quantification of Lung PET Images: Challenges and Opportunities [J]. J Nucl Med. 2017;58(2):201–7.
12. HARRIS RS. SCHUSTER D P. Visualizing lung function with positron emission tomography [J]. J Appl Physiol (1985). 2007;102(1):448–58.

13. LEDOULT E, MORELLE M, SOUSSAN M, et al. (18)F-FDG positron emission tomography scanning in systemic sclerosis-associated interstitial lung disease: a pilot study [J]. Arthritis Res Ther. 2021;23(1):76.
14. KIPRITIDIS J, HOFMAN M S SIVAS, et al. Estimating lung ventilation directly from 4D CT Hounsfield unit values [J]. Med Phys. 2016;43(1):33.
15. LEE Z, BERRIDGE MS. PET imaging-based evaluation of aerosol drugs and their delivery devices: nasal and pulmonary studies [J]. IEEE Trans Med Imaging. 2002;21(10):1324–31.
16. DOLOVICH M B, SCHUSTER DP. Positron emission tomography and computed tomography versus positron emission tomography computed tomography: tools for imaging the lung [J]. Proc Am Thorac Soc. 2007;4(4):328–33.
17. DOLOVICH M B. 18F-fluorodeoxyglucose positron emission tomographic imaging of pulmonary functions, pathology, and drug delivery [J]. Proc Am Thorac Soc. 2009;6(5):477–85.
18. GOEMINNE P C POLVERINOE. MCDONNELL M J, European Respiratory Society guidelines for the management of adult bronchiectasis [J]. Eur Respir J, 2017, 50(3).
19. MUNIR M, SETIAWAN H, AWALUDIN R, et al. Aerosolised micro and nanoparticle: formulation and delivery method for lung imaging [J]. Clin Transl Imaging. 2023;11(1):33–50.
20. BEHESHTI M, MOTTAGHY F M, PAYCHA F, et al. (18)F-NaF PET/CT: EANM procedure guidelines for bone imaging [J]. Eur J Nucl Med Mol Imaging. 2015;42(11):1767–77.
21. CHALMERS JD, HAWORTH C S, FLUME P et al. European Respiratory Society clinical practice guideline for the management of adult bronchiectasis [J]. Eur Respir J, 2025, 66(6).
22. WASSERTHAL J, BREIT H C, MEYER M T, et al. TotalSegmentator: Robust Segmentation of 104 Anatomic Structures in CT Images [J]. Radiol Artif Intell. 2023;5(5):e230024.
23. BAILEY D L, ESLICK E M, SCHEMBRI G P, et al. (68)Ga PET Ventilation and Perfusion Lung Imaging-Current Status and Future Challenges [J]. Semin Nucl Med. 2016;46(5):428–35.
24. PEREA L, FANER R, CHALMERS JD et al. Pathophysiology and genomics of bronchiectasis [J]. Eur Respir Rev, 2024, 33(173).

Figures

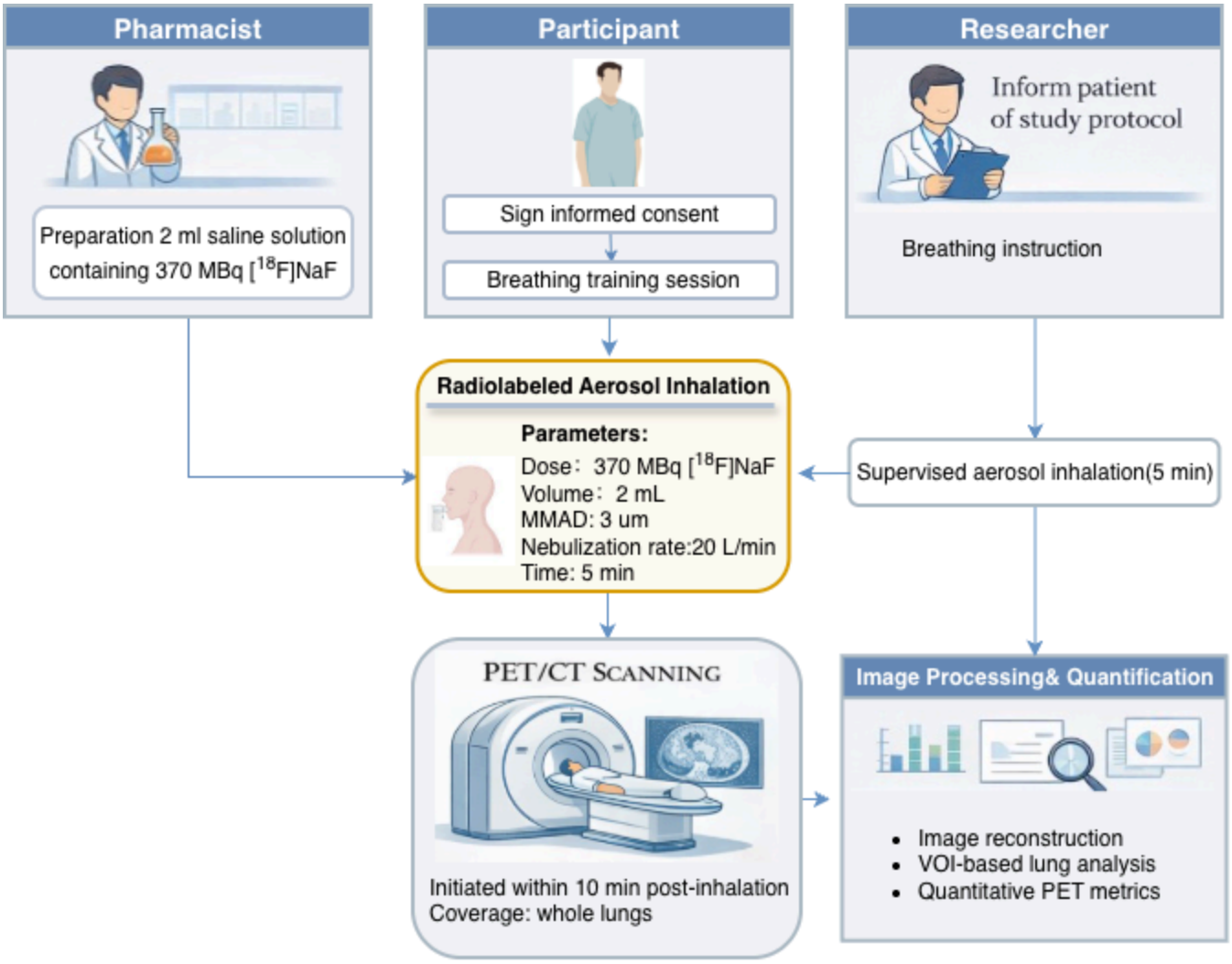


Figure 1

Imaging Protocol Flowchart for [^{18}F]NaF Nebulized Inhalation PET/CT

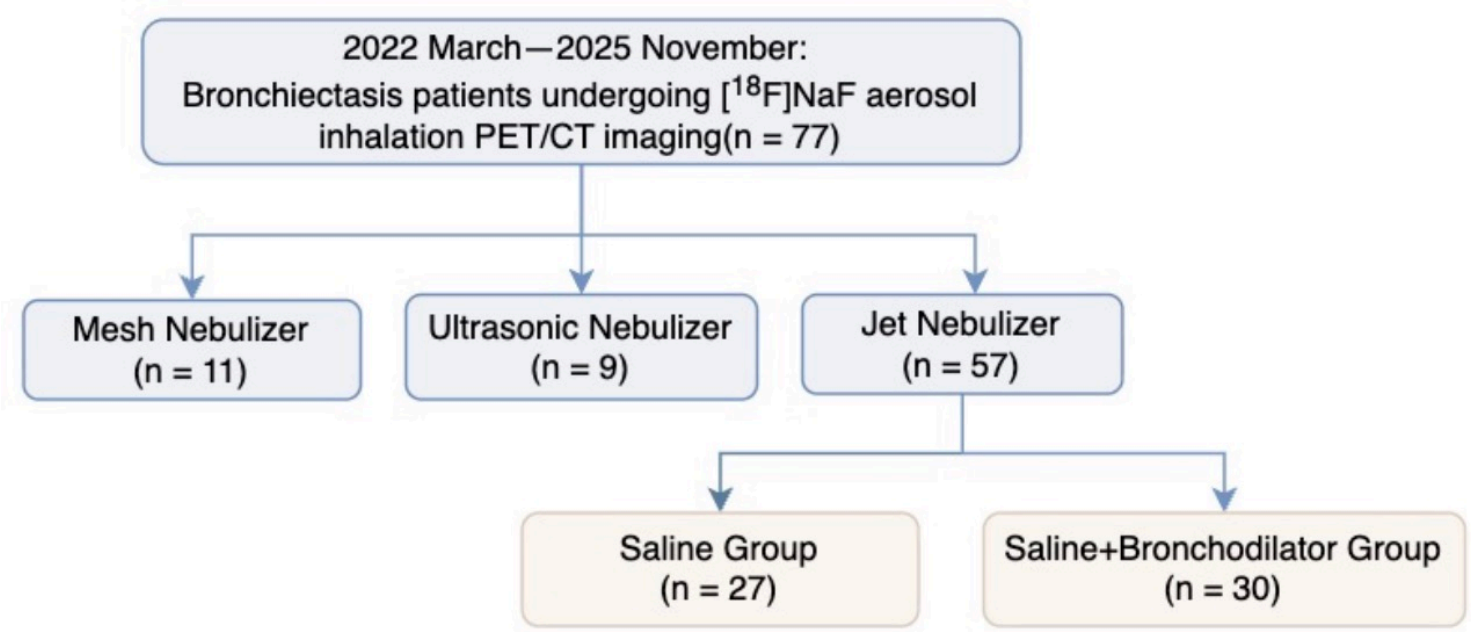


Figure 2

Flowchart of cohort enrollment and subgroup allocation

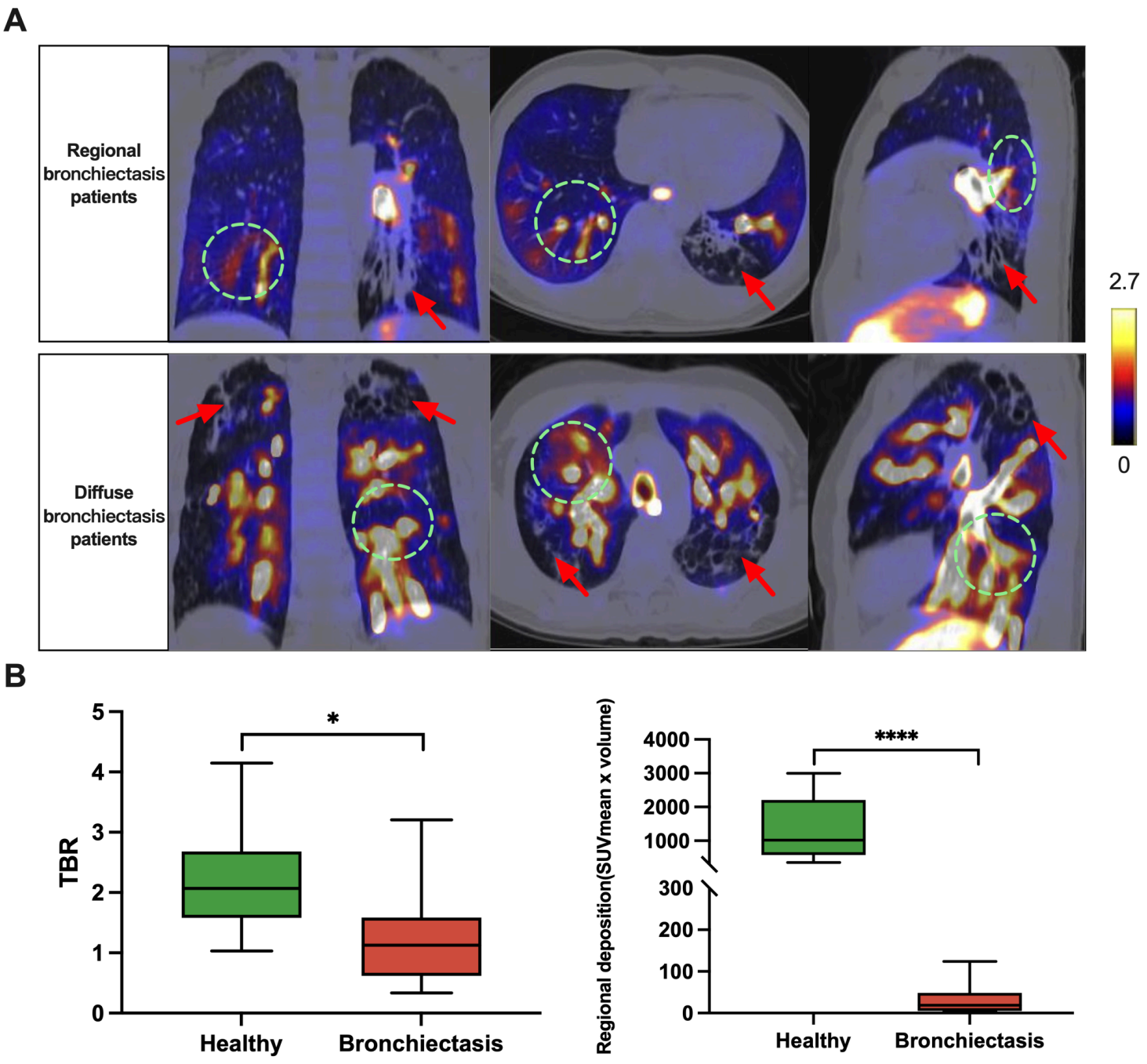


Figure 3

Reduced regional deposition of aerosolized [^{18}F]NaF in bronchiectatic lung regions. (A) Representative fused [^{18}F]NaF PET/CT images from patients with regional and diffuse bronchiectasis (Initial post-inhalation PET scan, 0 min). Green dashed circles indicate reference healthy lung regions, and red arrows indicate bronchiectatic regions, which show visually reduced tracer activity. (B) Comparison of regional aerosol deposition between Healthy and Bronchiectatic Lung Region.*P < 0.05; ****P < 0.0001

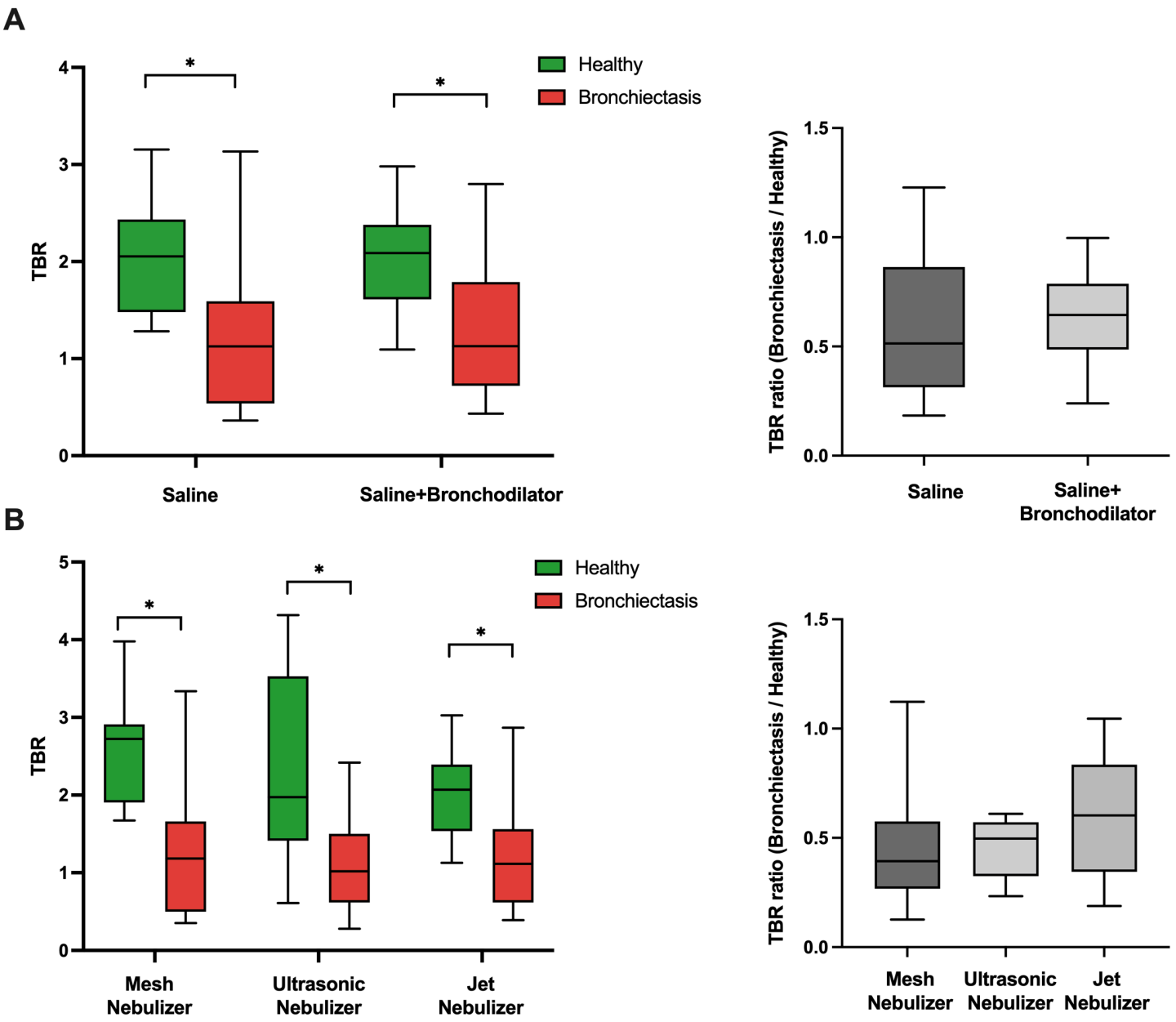


Figure 4

Persistently reduced bronchiectatic lung regions deposition relative to healthy lung region across medication regimens and nebulizer types. (A) TBR (mean ± SD) and TBR ratio (bronchiectasis/healthy) for saline vs saline plus bronchodilator. (B) TBR (mean ± SD) and TBR ratio for mesh, ultrasonic, and jet nebulizers. Green, healthy; red, bronchiectasis. *P < 0.05 (healthy vs bronchiectasis).

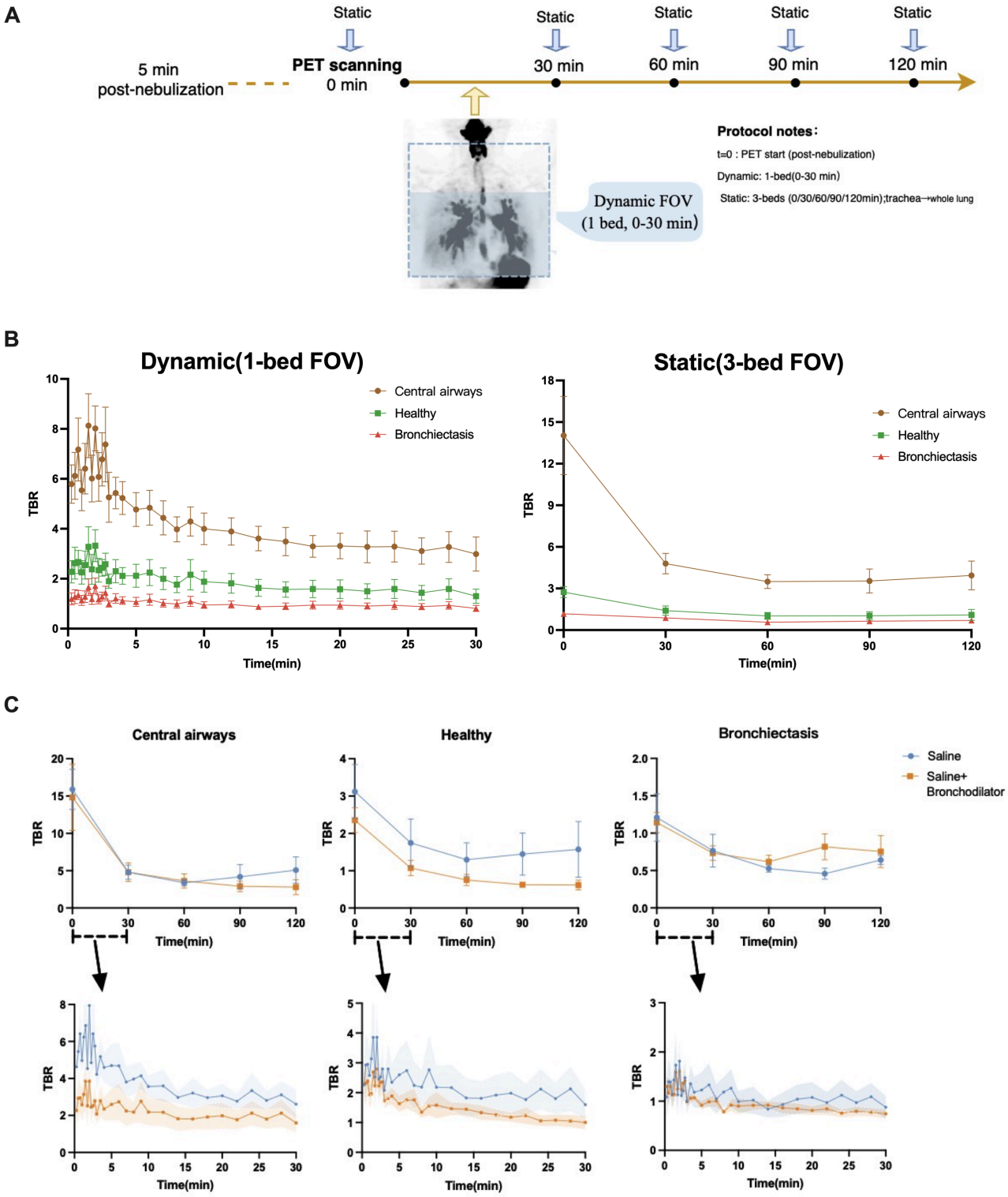


Figure 5

Regional [^{18}F]NaF aerosol PET/CT kinetics and regimen comparison (n=10). (A)Study imaging timeline and PET/CT acquisition time points. (B) TBR time–activity curves for central airways, healthy lung, and bronchiectatic regions(n=10, Jet nebulizer,including saline and saline plus bronchodilator group). (C) Regimen-specific curves (saline vs saline plus bronchodilator); In the saline group (n=5), 3 cases had mild ventilatory dysfunction and 2 cases were normal; In the saline plus bronchodilator group (n=5), 2

cases had mild ventilatory dysfunction and 3 cases were normal. No significant between-regimen differences in any region.

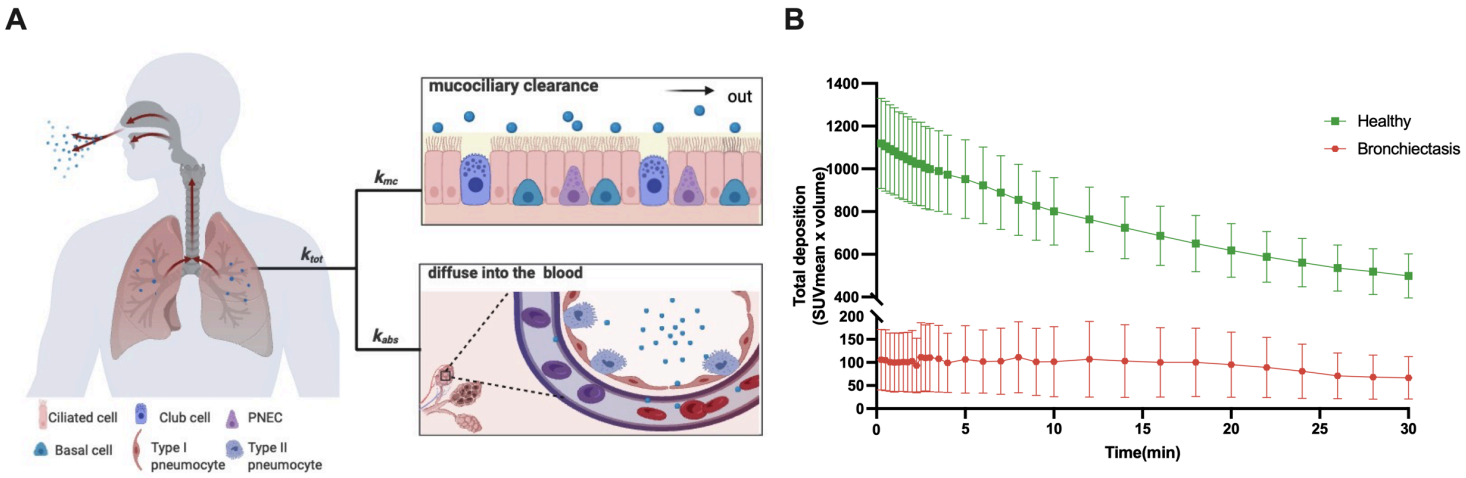


Figure 6

Dual-pathway clearance modeling of aerosolized [^{18}F]NaF PET. (A) Model schematic partitioning total clearance (k_{tot}) into mucociliary clearance (k_{mc}) and blood absorption (k_{abs}). (B) Dynamic total deposition (SUVmean×volume) over 0–30 min in healthy and bronchiectatic regions.

Supplementary Files

This is a list of supplementary files associated with this preprint. Click to download.

- Supplementary1.docx